Rotating Quarter-Wave Plate Stokes Polarimeter

Bachelorarbeit in Physik
von Sebastian Arnoldt

Angefertigt im Institut für Angewandte Physik

Vorgelegt der Mathematischen-Naturwissenschaftlichen Fakultät
der Universität Bonn

Oktober 2011

1. Gutachter: Prof. Dr. Dieter Meschede
2. Gutachter: Dr. Frank Vewinger

Contents

1 Introduction

In many physical applications, the ability to measure the polarization state of light is mandatory. Depending on the specifics of the set-up, there are numerous ways to construct measurement devices for the polarization state of light. All of these so called *polarimeters* are based on a common idea: modulating the intensity of a test signal with optical elements [6].

Dlugunovich et al. [6] divide polarization measurement techniques into static and dynamic. Static polarimeter set-ups work with multiple detectors and have no moving optical elements in the optical path. Dynamic methods, however, are based on moving optical elements in the optical path and make use of only one detector.

The advantage of dynamic polarimeter set-ups is that the state of polarization is measured with only one detector. This eliminates the need to develop sophisticated error reduction algorithms that arise in static multichannel polarimeters [11].

The aim of this thesis is to design, construct and test a rotating quarter wave plate Stokes polarimeter that is capable of measuring all polarization states of light. The insights gained from this polarimeter set-up should provide a foundation for the development of a dynamic polarization control in the few-atom quantum systems of the Quantum Technologies group at the Institut für Angewandte Physik at Bonn University.

2 Theoretical Considerations

The state of polarization of electromagnetic (EM) radiation can be expressed by the *Stokes parameters*. This thesis uses the definition of the Stokes parameters according to [8] :

$$\begin{aligned} S_0 &= E_x E_x^* + E_y E_y^* \\ S_1 &= E_x E_x^* - E_y E_y^* \\ S_2 &= E_x E_y^* + E_y E_x^* \\ S_3 &= i(E_x E_y^* - E_y E_x^*) \end{aligned} \tag{1}$$

where $E_x = E_{0x} exp(i\delta_x)$ and $E_y = E_{0y} exp(i\delta_y)$ are the complex amplitudes of the electric field in the plane transverse to the propagation direction of the EM wave and $\delta = \delta_x - \delta_y$ is the phase difference between E_x and E_y. Arranging the Stokes parameters in a column matrix defines the so-called *Stokes vector* S:

$$S = \begin{pmatrix} S_0 \\ S_1 \\ S_2 \\ S_3 \end{pmatrix} \tag{2}$$

From Eq. 1 and Eq. 2 the Stokes vectors for any polarization state can be calculated. For instance, the Stokes vectors of linear vertically polarized (LVP) light, right circular polarized (RCP) and elliptical polarized light of some arbitrary state are[8]:

$$\vec{S}_{\mathrm{LVP}} = \begin{pmatrix} 1 \\ -1 \\ 0 \\ 0 \end{pmatrix} \qquad \vec{S}_{\mathrm{RCP}} = \begin{pmatrix} 1 \\ 0 \\ 0 \\ 1 \end{pmatrix} \qquad \vec{S}_{\mathrm{Ellipt}} = \begin{pmatrix} 1 \\ 0.33 \\ 0.33 \\ 0.34 \end{pmatrix} \tag{3}$$

As the Stokes formalism is an intensity formulation of the polarization, S_0 is equivalent to the total intensity of a light beam and S_1 to the amount of

linear horizontal polarization (LHP) or LVP. S_2 stands for the amount of linear +45° (+45LP) or linear -45° (-45LP) polarization. Finally, S_3 is equal to the amount of right or left circular (RCP or LCP) polarization in a light beam. With the Stokes parameters, the *Degree of Polarization* (DOP) is defined as the ratio of the sum of the intensity of the polarized light and the total intensity of a light beam [8]:

$$DOP = \frac{\sqrt{S_1^2 + S_2^2 + S_3^2}}{S_0} \; 0 \leq DOP \leq 1 \tag{4}$$

Since the DOP should not be greater than 1 and should be equal to 1 for completely polarized light, it will be used as a measure of goodness for the results of this thesis.

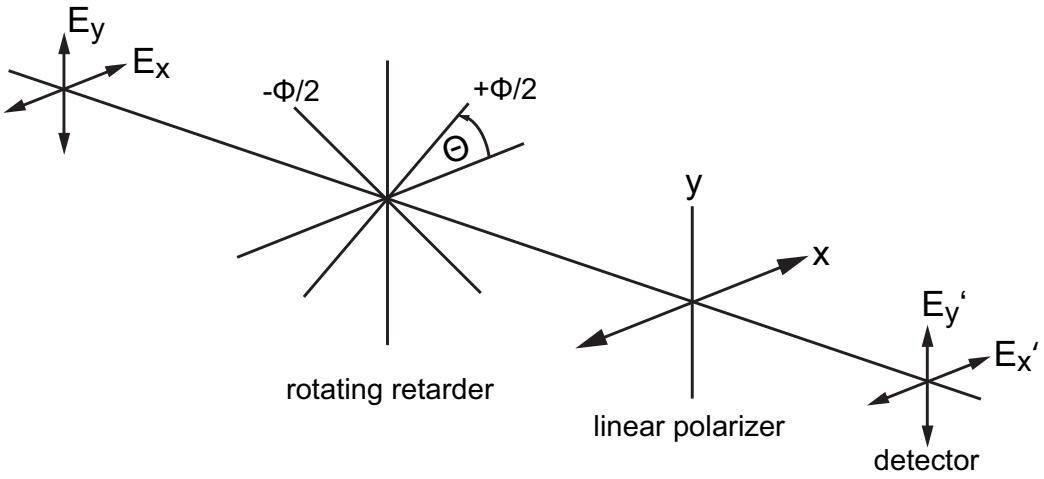

Figure 1: Stokes Polarimeter consisting of a rotating retarder plate, a fixed linear polarizer and a detector ([8], p.99).

Following [8], the Stokes paremeters of a test signal can be measured with the set-up shown in Fig. 1 above. Here, a test signal is first modulated by a rotating quarter wave plate and then passes through a linear polarizer. The measured intensity $I(\Theta)$ at the detector as a function of the rotation angle Θ of the retarder is calculated using Mueller calculus:

$$I(\Theta) = \frac{1}{2} \cdot [A - B \cdot \sin(2\Theta) + C \cdot \cos(4\Theta) + D \cdot \sin(4\Theta)], \tag{5}$$

where

$$\begin{aligned} S_0 &= A - C \\ S_1 &= 2C \\ S_2 &= 2D \\ S_3 &= B. \end{aligned} \tag{6}$$

Eq. (5) is a truncated Fourier series, whose coefficients are:

$$\begin{aligned} A &= \frac{1}{\pi}\int_0^{2\pi} I(\Theta)\,\mathrm{d}\Theta \\ B &= \frac{2}{\pi}\int_0^{2\pi} I(\Theta) sin(2\Theta)\,\mathrm{d}\Theta \\ C &= \frac{2}{\pi}\int_0^{2\pi} I(\Theta) cos(4\Theta)\,\mathrm{d}\Theta \\ D &= \frac{2}{\pi}\int_0^{2\pi} I(\Theta) sin(4\Theta)\,\mathrm{d}\Theta \end{aligned} \tag{7}$$

Fig. 2 below shows plots of the theoretically expected intensity modulation seen by the detector of the polarimeter for light in the polarizations states of Eqs. (3) . This is done by plugging Eqs. (3) into Eq. (5) and plotting $I(\omega t) = I(\Theta)$ from 0 to 2π, where Θ is the rotation angle of the quarter wave plate (QWP).

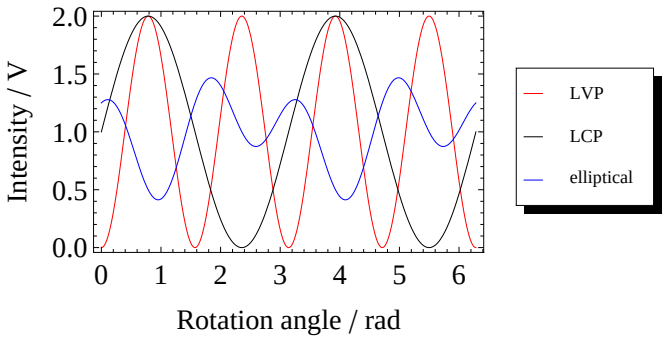

Figure 2: Modulated intensity signals as seen by the detector of the rotating QWP Stokes polarimeter.

3 The Rotating Quarter-Wave Plate Stokes Polarimeter Set-Up

The set-up of the rotating quarter-wave plate polarimeter is shown in Fig. 3 below. Light from a 852 nm diode laser passes through a Faraday-isolater and enters an optical attenuator, consisting of a half-wave plate (HWP) and a polarizing beam splitter (PBS). The PBS splits the signal into two beams, that are called *test signal* and *trigger signal*. The test signal passes through the device under test (DUT) and is then modulated by a continuously rotating quarter-wave plate (QWP), which is mounted in a self-designed rotation mount. At the heart of the rotation mount is a double row industry ball bearing (SKF YAT 205), which has been pressed into an aluminum mount by the mechanical work shop.

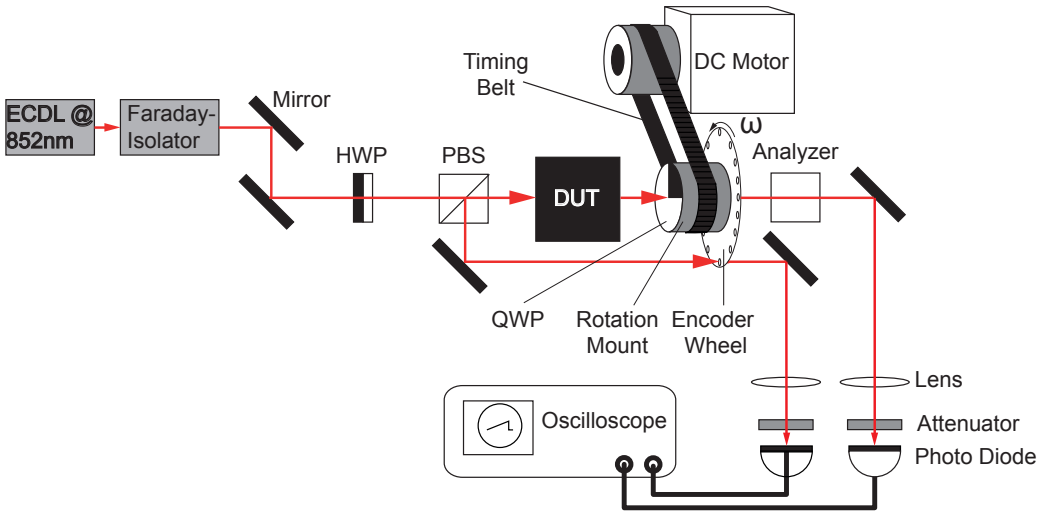

Figure 3: Set-up of the rotating QWP Stokes polarimeter.

Leaving the rotation mount, the test signal passes through an analyzer and is focussed onto an amplified photo diode (PD1) by a lens. Between the photo

diode and the lens, the attenuater ensures that the photo diode measures the test signal in the linear range.

Leaving the PBS, the trigger signal is chopped by the holes of an encoder wheel that has 64 evenly spaced holes and is held by the same rotation mount as the QWP. The encoder wheel is fixed to the rotation mount with epoxy adhesive and is made of an old hard drive disk. The holes have been drilled into the encoder wheel by the work shop with a precision in the micro meter range. One of the holes is reduced in diameter with tape and is referred to as *reference hole* in the following.

Behind the encoder wheel, an amplified photo diode (PD2) picks up the trigger signal, where the trigger signal is again focussed by a lens and passes through an attenuator. The signals created by PD1 and PD2 are recorded with a Tektronix DPO 4104 digital oscilloscope at a sampling rate of 250kS/ s since no data acquisition box with sufficiently high sampling rate is available.

The rotation mount is driven by an industrial DC motor from ebmpabst (type: BCI 63.55), that is connected to the mount via a timing belt. The motor is connected to a commercial closed-loop speed control circuitry, which stabilizes the motor at low rotation frequencies. Since the QWP and the encoder wheel are held by the same rotation mount, they are rotating at the same frequency.

3.1 Data Sampling

As shown in the introductory part, the determination of the Stokes parameters is based on Fourier transforming the recorded test signal. In the data analysis, this is done with the Discrete Fourier transform algorithm in Mathematica [9]. This means, that the recorded test signal needs to be sampled, which is the task of the encoder wheel and subsequently Mathematica. After the sampling process, the phase shift between the trigger and the test signal ϕ_{TT} needs to be determined in order to get the correct results from the Fourier transform. ϕ_{TT} is determined as shown in Fig. 4 below, where a small piece of the recorded trigger and test signal in the LVP state are depicted.

The following procedure is carried out in Mathematica. Using the trigger

level, the position of the rising part of the reference hole $t_{\mathrm{ref_1}}$ is determined on the time axis. The ticks on the time axis are defined by the sampling rate at which the oscilloscope records the data. Since the reference hole has been aligned with the fast axis of the QWP before, $t_{\mathrm{ref_1}}$ provides a coarse position of the fast axis of the QWP. Second, the position of the minimum of the test signal t_{minTest} in the surrounding of the reference hole is determined on the time axis by non-linear curve-fitting in Mathematica.

This is done because the test signal is in the LVP state, which is why the polarimeter records a minimum intensity at the location of the axes of the QWP. Since the reference hole is aligned with the marked fast axis of the QWP in the calibration of the polarimeter, the minimum of the recorded test signal in the LVP state close to the reference hole is equivalent to the position of the fast axis on the time scale.

As a next step, the phase shift ϕ_{TT} between the reference hole on the encoder wheel and the fast axis of the QWP is calculated as

$$\phi_{\mathrm{TT}} = t_{\mathrm{ref_1}} - t_{\mathrm{minTest}}. \tag{8}$$

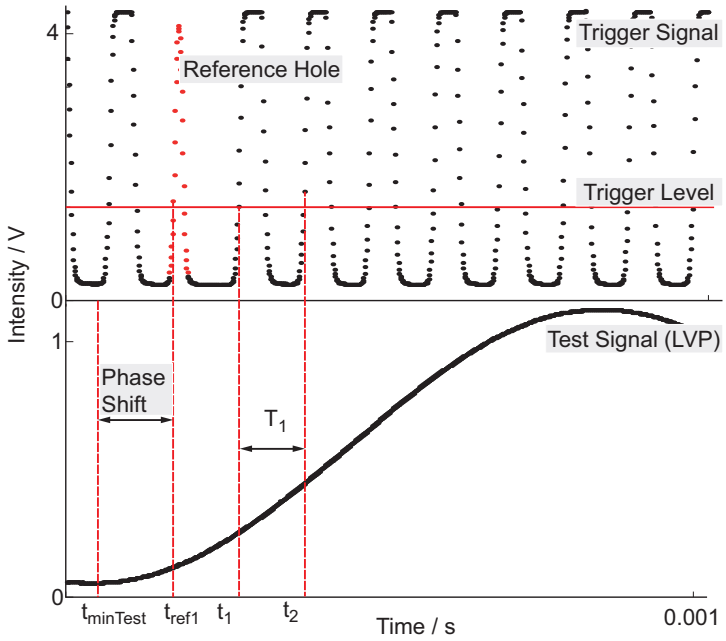

Figure 4: Phase Shift between Trigger Signal and Test Signal.

After ϕ_{TT} has been determined, the test signal is sampled. This is done as follows: the first data point of the sampled signal is taken from the test signal at the position $t_{\mathrm{ref_1}} + \phi_{\mathrm{TT}}$ on the time axis. Next, the second point of the sampled signal is taken from the position of the second hole on the encoder wheel plus the phase shift $t_{\mathrm{Trig2}} + \phi_{\mathrm{TT}}$. While this is done, ϕ_{TT} is dynamically corrected as a function of the motor speed, as will be shown in Sec. 3.3.7. This procedure is repeated for all 64 encoder wheel holes, which corresponds to one full rotation of the QWP. One period of a sampled LVP signal from real measurement data is depicted in Fig. 5 below.

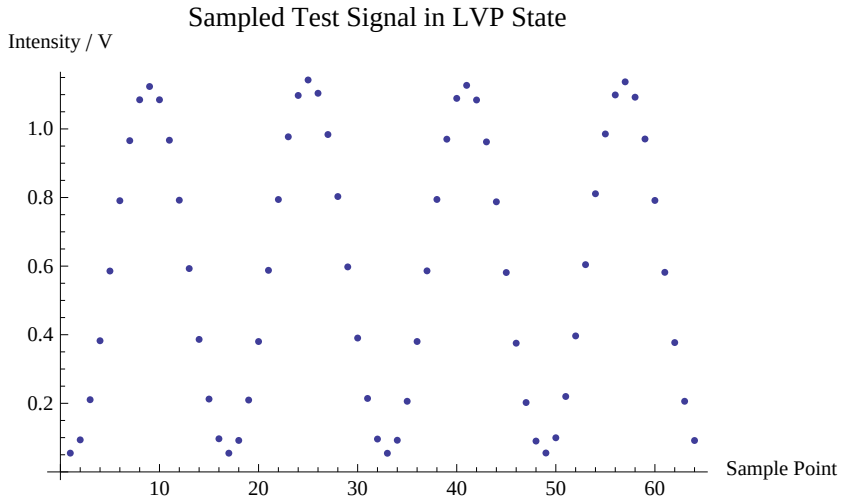

Figure 5: Signal sampled with the encoder wheel from one full rotation of the QWP.

After the sampling process, the sampled signal is Fourier transformed, which provides the DC, $\cos(4\omega)$, $\sin(4\omega)$ and $\sin(2\omega)$ terms needed to calculate the Stokes parameters with Eq. 6. In order to get meaningful results from the Fourier transform, the number of samples per period must be a multiple of four, which explains the number of holes on the encoder wheel. For practical reasons, test signals of the length of 7 full rotation periods of the QWP are analyzed in the Data Analysis Section.

3.2 Procedure

3.2.1 Calibrating the Polarimeter

First, the QWP and the DUT are removed from the polarimeter set-up. Switching on the laser and rotating the analyzer, the intensity of both signals are checked to be in the linear range of PD1 and PD2. During the calibration process, intensity adjustments of both signals can be made by varying the laser power directly, by using the optical attenuator in the set-up and by inserting filters as shown in fig. 3 above.

Next, a polarizer that creates light in the LVP state is placed as a DUT behind the beam splitter and the output of PD1 is connected to a digital volt meter (DVM). Now the analyzer is carefully rotated until the intensity of the test signal is minimal on the DVM. The rotation mounts of the DUT and the analyzer are then locked at these positions. Subsequently, the QWP is placed into the rotation mount and fixed in such a way, that its fast axis is aligned with the reference hole of the encoder wheel as tightly as possible.

3.2.2 True Retardance of the Wave Plate

As will be shown in the Data Analysis part (Sec. 3.3), it is crucial to know the true retardance δ of the rotating QWP. Therefore the true retardance of the rotating QWP is determined with the crossed polarizer method suggested by Goldstein [8, pp. 124–128] , which is illustraded in Fig. 6 below.

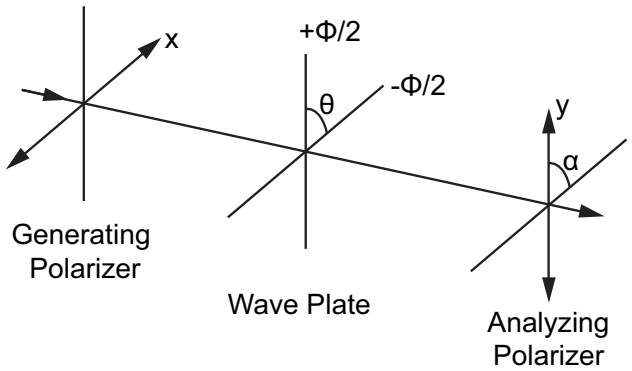

Figure 6: Crossed polarizer method to determine the phase shift of a wave plate. $+\phi/2$ and $-\phi/2$ are the fast and slow axes of the wave plate [8, p.125].

In this method, the wave plate is inserted between two crossed polarizers that are mounted in precision rotation mounts. When the angle between the fast axis of the wave plate and the x direction is at $\Theta = 45°$, the intensity behind the analyzer can be expressed as a function of the retardance δ of the wave plate and the angle α of the analyzer transmission axis with the x direction:

$$I(\alpha, \delta) = \frac{I_0}{4}(1 + \cos(\delta)\cos(2\alpha)) \tag{9}$$

Measuring the intensity at $\alpha = 0°$ and $\alpha = 90°$, the cosine of the phase shift is calculated from Eq. 9:

$$\cos(\delta) = \frac{I(0°, \delta) - I(90°, \delta)}{I(0°, \delta) + I(90°, \delta)} \tag{10}$$

The advantage of this method is that it is independent of the source intensity of the laser beam. Moreover, the use of high precision rotation mounts makes this measurement relatively precise. To determine the phase shift of the wave plates used in this set-up, the above measurement is repeated ten times for each wave plate to determine the measurement uncertainty $\Delta\delta$ for δ.

3.2.3 Wave Plate Ripple

Another preliminary measurement is the recording of the so called *wave plate ripple*, which describes an observed modulation in the recorded intensity when the QWP is rotated and there is no optical element between the QWP and the photo diode. The wave plate ripple of the QWP can be observed with the set-up shown in fig. 7 below. Here, light in the LVP state is launched into a rotating QWP. Behind the rotating QWP, the intensity of the signal is measured with an amplified photo diode. The wave plate is rotated by the DC motor as in the polarimeter set-up.

According to [2], [5] and [4], the ripple may be explained by assuming that a wave plate consists of several Fabry–Pérot etalons. In an air-spaced wave plate, for instance, two of these etalons are formed by the crystal quartz plates themselves. The third etalon consists of the two quartz plates and the

air space between them. The wave plate ripple is thought to cause an error in the measurement of the Stokes parameters [5]. A detailed analysis of this problem is given in [2].

Hough [5] suggests, that the observed wave plate ripple is minimized when cemented or optically contacted wave plates are used. For this reason,the spectra of two wave plates are recorded. One of the wave plates is a zero-order air-spaced QWP from LensOptics (type: W4Z20-852). The other QWP is an unknown QWP found in the laboratory that is not air-spaced. It will be referred to as WP1 in the following.

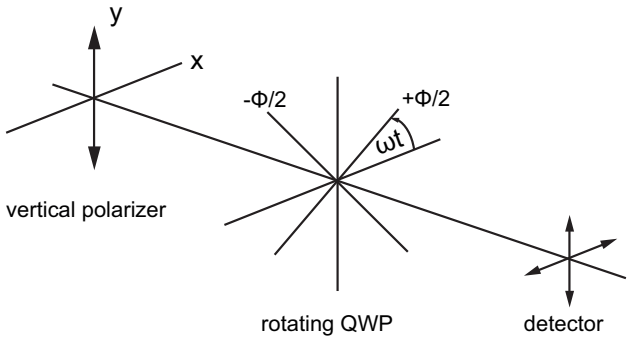

Figure 7: Set-up for observing wave plate ripple.

The spectra of both QWPs are recorded with the polarimeter set-up, where the analyzer is removed. The lights in the laboratory need to be turned off during this measurement. The signals recorded have a length of 20 full rotations of the QWP at a sampling rate of 250 kS/s. The LVP polarizer remains in the set-up as a DUT from the calibration, leaving the position of its transmission axis unchanged. The spectrum of a wave plate should be taken right before or after the measurement, since it changes over time [12]

3.2.4 Taking the Polarization Measurement

Having completed the preliminary measurements and the calibration of the polarimeter, the actual polarization measurements are taken. To reduce the noise picked up by the photo diodes, all measurements are taken with the lights turned off in the laboratory. As DUTs, test signals in the LVP,-45LP

and LHP polarization state are used. These polarizations are created by using a combination of a polarizer and a HWP, where the polarizer is mounted on a precision rotation mount. The theoretically expected normalized Stokes vectors of these measurements are $S_{\mathrm{LVP}} = (1, -1, 0, 0)^T$, $S_{\text{-45LP}} = (1, 0, -1, 0)^T$ and $S_{\mathrm{LHP}} = (1, 1, 0, 0)^T$. Here, normalized Stokes vector means that each parameter of the Stokes vector is divided by the Stokes parameter S_0. For all of these DUTs, the expected $DOP = 1$.

For each measurement, test and trigger signals of the length of 2 million data points are recorded with the oscilloscope at a sampling rate of 250 kS/s and low rotation frequencies of the DC motor. These signals are then chopped into smaller pieces that have a length of 7 rotation periods of the QWP. From these smaller pieces, signals are randomly picked and analyzed. All measurements are done with the ZO-WP and WP1 and the above DUTs. The recorded signals are then evaluated using Mathematica. For the statistical analysis, data sets of ten single measurements are extracted from the long recordings for each DUT. Each of these single measurements is again 7 periods long.

3.3 Data Analysis

The error sources for this set-up can be divided into systematic errors, measurement errors and random fluctuations of parameters. Systematic error sources are the error in the retardance of the QWP, wave plate ripple, analyzer misalignment, misalignment of the DUT and the noise of the recording electronics [6, 5, 11]. Parameters that fluctuate randomly are the rotation frequency of the motor, the laser intensity and the wobbling of the rotating wave plate in the rotation mount [11]. All calculations and analysis in the following chapter are done with Mathematica. For all calculations below, the functions *Mean* and *StandardDeviation* in Mathematica are used to calculate the mean and the standard deviation. If not stated otherwise, Gaussian error propagation is used for the calculation of errors. The term *single measurement* refers to the determination of the Stokes parameters from a test signal, whose length is 7 rotation periods of the QWP.

3.3.1 Electronics Offset and Signal To Noise Ratio

As a first step, the offset of the readout electronics needs to be substracted from all analyzed test signals. Since the readout is done with a digital oscilloscope, the offeset needs to be monitored closely before, between and after each measurement. The signal to noise ratio (SNR) of the analyzed signals is SNR= 0.002.

3.3.2 Retardance Error

Since the specified operational range of the wave plate is not met in this particular set-up, the true retardance of the rotating QWP differs from the specified 90°. The resulting systematic error in the Stokes parameters can be corrected, by recalculating Eq. 6 with the true retardance δ of the QWP [11]. From this, the corrected Stokes parameters are:

$$\begin{aligned} S_0(\delta) &= A - C/\tan^2(\delta/2) \\ S_1(\delta) &= 2C/2\sin^2(\delta/2) \\ S_2(\delta) &= 2D/2\sin^2(\delta/2) \\ S_3(\delta) &= B/\sin(\delta) \end{aligned} \tag{11}$$

The true retardance δ is determined experimentally for the ZO-WP and WP1 with the crossed polarizer method described in Sec. 3.2 above. The results are shown in Tab. 1 below where $\Delta\delta$ is the standard deviation of ten measurement results of δ.

Table 1: δ for ZO-WP and WP1.

	δ / °	$\Delta\delta$ / °
ZO-WP	85.3	±0.3
WP1	87.7	±0.3

From the theory, the effect of the correction of δ on the Stokes parameters is expected to be most dramatic in the -45LP state. This expectation is met in the measurements. Tab. 2 shows the effect of the correction of δ on a single -45LP measurement with the ZO-WP. The measurement error is a cumulated error from the retardance, the analyzer misalignment and the sampling error, as will be explained below.

Table 2: Correction of δ in $-45LP$ Measurement with ZO-WP.

	Uncorr. Meas. Val. / V	Corr. Meas. Val. / V	Meas. Err. / V
S_0	1.4418	1.4453	±0.0279
S_1	-0.0419	-0.0454	± 0.0260
S_2	-1.3388	-1.4528	± 0.0156
S_3	-0.0158	-0.0159	± 0.0050
DOP	0.9291	1.0057	± 0.0433

In addition to the correction of δ, the measurement error $\Delta\delta$ of the true

retardance needs to be considered. This is done by recalculating Eq. 11 at the upper and lower limit of $\delta \pm \Delta\delta$. For instance, the measurement error for S_0 due to the measurement error of δ is calculated as $\Delta S_0^{\text{up}} = S_0(\delta+\Delta\delta)-S(\delta)$ and $\Delta S_0^{\text{low}} = S_0(\delta-\Delta\delta)-S(\delta)$. For the above single -45LP, this measurement error is shown in Tab. 3 below. It makes up one part of the cumulated measurement error in Tab. 2 above.

Table 3: Measurement Error in Stokes parameters due to $\Delta\delta$.

	Meas. Val. / V	Meas. Err. / V
S_0	1.4418	± 0.0003
S_1	-0.0419	± 0.0003
S_2	-1.3388	± 0.0082
S_3	-0.0158	± 0.0000

The above data shows the dramatic effect that the correction of δ has on the measurement results. The S_2 parameter of the -45LP measurement is reduced by almost 10 % by the δ correction. The relative measurement error $\Delta S_i^{\text{up/low}}/S_i$, however is below 1 %. The measurement error $\Delta S_i^{\text{up/low}}$ caused by $\Delta\delta$ will be included in all calculations from now on and will be listed in the cumulated measurement error of all following tables.

3.3.3 Analyzer Misalignment

The misalignment of the polarimeter's analyzer is another source of systematic error in the measurement of the Stokes parameters [7, 3]. In analogy to the retardance error, the effect of this error on the Stokes parameters is shown by recalculating Eq. 6 at the angle α between the transmission axis of the analyzer and the x direction [7]:

$$
\begin{aligned}
S_0(\alpha) &= S_0 + S_2 \sin(2\alpha) \\
S_1(\alpha) &= S_1 \cos(2\alpha) - S_2 \sin(2\alpha) \\
S_2(\alpha) &= S_2 \cos(2\alpha) + S_1 \sin(2\alpha) \\
S_3(\alpha) &= S_3 \cos(2\alpha)
\end{aligned} \tag{12}
$$

As shown in Sec. 3.2 , α can be adjusted to $\alpha = (0.0 \pm 0.2)^\circ$ in the polarimeter set-up. In analogy to the measurement error of the true retardance, Eq. 12 are eavluated at the upper and lower limit of $(\alpha \pm \Delta\alpha)$. For the same − 45LP measurement as above, this produces the measurement errors in the Stokes parameters shown in Tab. 4 below. The relative measurement error $\Delta S_i^{\mathrm{up/low}}/S_i$ due to $\Delta\alpha$ is below 1 %. The measurement error caused by $\Delta\alpha$ will be included in all calculations from now on and will be listed in the cumulated measurement error of all following tables.

Table 4: Measurement Error in Stokes parameters due to $\Delta\alpha$.

	Meas. Val. / V	Meas. Err. / V
S_0	1.4418	±0.0093
S_1	-0.0419	± 0.0093
S_2	-1.3388	± 0.0003
S_3	-0.0158	± 0.0000

3.3.4 Reference Polarizer and DUT Misalignment

Another measurement error is made when the DUT is calibrated. The DUT in this project are polarizations in the LVP, -45LP and LHP state. These are created by placing a polarizer as DUT at the corresponding angles β with the x direction. With the precision rotation mounts, β can be calibrated with an estimated error of $\Delta\beta = 0.2^\circ$. This means, that the above measurement error for α is doubled in the -45LP and LHP state, since it does not matter for the theoretical calculation of the error, whether the analyzer

of the polarimeter or the generating polarizer is rotated by 0.2°. Since the polarimeter is calibrated with the LVP state, there is no additional $\Delta\alpha$ for the LVP state. The measurement error due to $\Delta\beta$ will be included in all calculations from now on and will be listed in the cumulated measurement error of all following tables.

3.3.5 Motor Jittering

Errors in the measurement of the Stokes parameters due to random motor jittering occur, when the test signal is sampled using the trigger signal. Measurements of the rotation frequency show, that the DC motor used in this set-up runs smoother at lower frequencies than at higher frequencies. This shows that the closed-loop speed control of the DC motor is working correctly.

To analyze the stability of the motor at low frequencies, a 4 s sample of the trigger signal is recorded at a sample rate of 250 kS/s s and at a rotation frequency $f \approx 35$ Hz. Next, the time differences $T_i = t_i - t_{i+1}$ between the adjacent rising parts of the trigger signal are calculated. Then, the Allan variance of the T_i is calculated using Eq. 13 in the Appendix. Fig. 8 below shows a double logarithmic plot of the square root of the Allan variance for increasing subensembles of the T_i. This plot shows that the T_i are not stable over time and have periodic fluctuation in the rotation speed. This may be attributed to jittering in the motor speed and to the fact, that the encoder wheel is not fixed perfectly to the center of the rotation mount.

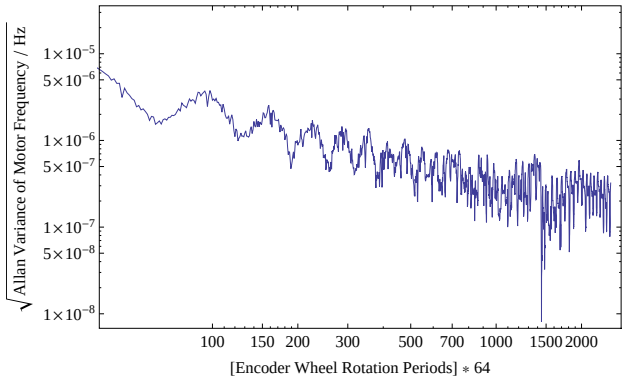

Figure 8: Allan variance of length of rotation periods T_i.

Consequently, the effects of motor jittering need to be taken into account, when the test signal is sampled. Since the encoder wheel and the rotating wave plate are physically attached to the same rotation mount, the error made in the sampling process due to the motor jittering is minimized. However, a small error remains, since the alignment of the fast axis of the QWP and the reference hole is not perfect. As a result, the phase shift ϕ_{TT} between the fast axis of the QWP and the reference hole will change as a function of time. Moreover, a systematic error may be introduced by the imperfect alignment of the encoder wheel with the rotation mount.

3.3.6 Estimation of the Sampling Error

In a 7 period long signal, that is recorded at the same settings as the signal above, the fluctuations in the T_i around the mean of the T_i of the trigger signal are roughly 5%. The phase shift ϕ_{TT} is found by fitting a non-linear curve through the minimum of the LVP signal in the vicinity of the reference hole. It can be determined with an accuracy of 1% of the mean of the T_i. From this, the uncertrainty in finding the correct ϕ_{TT} is roughly estimated to be $\Delta\phi_{TT} = 6\%$ in terms of the mean width of the T_i in the analyzed signal.

This uncertainty translates into an error of the value that is sampled from the test signal. This error is estimated by taking the value of the test signal at a position, that is shiftet by the amount $\Delta\phi_{TT} \cdot T_{\mathrm{mean}}$ on the time axis and comparing it to the value, that would be sampled at T_{mean}. This is done

at a steep slope of the cosine of the LVP signal. The error produced in the selection of the right point to be sampled is then $\Delta_{\text{sample}} = \pm 0.011$ V.

Since the calculated Fourier coefficients are proportional to the values of the sampled signal, the measurement error of the A,B,C and D coefficient is roughly estimated to be 11 mV from the above argumentation. Using Gaussian error propagation and Eq.7 for the S_0, S_1, S_2 and S_3 parameters, the estimation translates into the following measurement errors: $\Delta S_0^{\text{sample}} =$ 19 mV, $\Delta S_1^{\text{sample}} = 16$ mV, $\Delta S_2^{\text{sample}} = 16$ mV $\Delta S_3^{\text{sample}} = 11$ mV. This should only be understood as a rough estimate of the measurement error due to the sampling process. A more detailed calculation of this error would be time-consuming and exceed the scope of this thesis. The above Δ_{sample} is checked with the measurement data. For this purpose the values of the minima and the maxima in the sampled signals are compared to their corresponding values in the measurement data. This comparison shows that the sampled data is in very good agreement with the estimated $\Delta_{\text{sample}} = \pm 0.011$ V.

3.3.7 Mottor Jitter Correction

An approach to correct the motor jitter from the analyzed data is introduced in the following. The idea is to determine the phase shift ϕ_{TT} and the corresponding $T_{\text{ref}} = t_{\text{ref1}} - t_{\text{ref1-1}}$ in the above 7 period long data set. With the fixed T_{ref} and ϕ_{TT} , the corrected phase shift for each sample point is calculated as $\phi_i = T_i \cdot \frac{\phi_{\text{TT}}}{T_{\text{ref}}}$ for each sample point. The measurement error produced by this method is estimated under the assumption, that the T_i and T_{ref} are more or less static and can be determined with a relative error of 1%. Using these assumptions, the maximum error of ϕ_{TT} is estimated to be $\Delta\phi = 2\%$ in terms of the T_{mean} of the signal. In analogy to the previous section, this results in an error $\Delta'_{\text{sample}} = \pm 0.005$ V, which will be used as an measurement error estimate for the measured Fourier coefficients. Thus, the measurement errors for the Stokes parameters are $\Delta S_0^{\text{sample'}} = 9$ mV, $\Delta S_1^{\text{sample'}} = 7$ mV, $\Delta S_2^{\text{sample'}} = 7$ mV $\Delta S_3^{\text{sample'}} = 5$ mV. The measurement error $\Delta S_i^{\text{sample'}}$ will be included in all calculations from now on and will be listed in the cumulated measurement error of all following tables.

Fig. 9 below shows the effects of the motor jitter correction on the measurement of the Stokes parameters. The left side of Fig. 9 shows the results of ten single measurements of S_2 of light in the LVP state. The measurements are done with the ZO-WP. Each single measurement is a recording of 7 rotation periods of the ZO-WP at a sample rate of 250kS /s and a motor frequency of $f \approx 35Hz$. The error bars for each single measurement are the cumulated measurement errors of the true retardance of the ZO-WP, the measurement error of the analyzer misalignment, and the sample measurement error as described above. Moreover, the mean of the ten measurement values and the corresponding standard deviation are shown on both sides of Fig. 9.

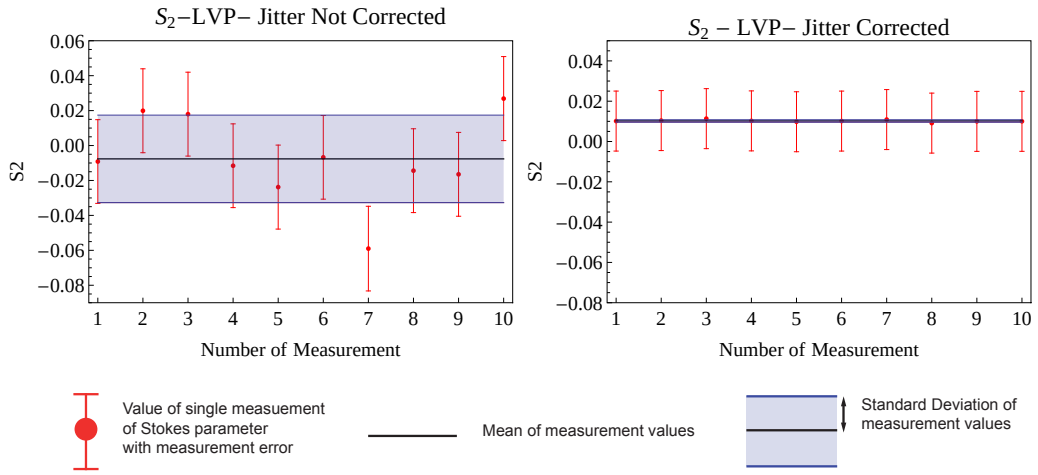

Figure 9: Effects of Motor Jitter Correction on Measurement Results of S_2

Comparing the left and right side of Fig. 9, a significant reduction in the standard deviation is observed after the motor jitter correction is applied to the data set.

The effect of the jitter correction on the standard deviation of all Stokes parameters of the above data set is shown in Tab. 5 above. Here, the mean measurement value is the mean value of the ten independent single measurement results from the above data set. Since the measurement errors of each Stokes parameter vary on a small scale between the ten measurements, their mean is given as mean measurement error. The standard deviation is the

Table 5: Motor Jitter Correction - LVP

	Jitter Not Corrected			Jitter Corrected		
	Mean Meas. Value / V	Mean Meas. Error / V	Std. Dev. / V	Mean Meas. Value / V	Mean Meas. Error / V	Std. Dev. / V
S_0	1.2248	±0.0261	0.0004	1.2178	±0.0160	0.0002
S_1	-1.2293	±0.0231	0.0251	-1.2161	±0.0140	0.0006
S_2	-0.0076	±0.0240	0.0251	0.0102	±0.0149	0.0006
S_3	0.0092	±0.0110	0.0001	0.0078	±0.0050	0.0005
DOP	1.0039	±0.0323	0.0002	0.9987	±0.0196	0.0002

calculated standard deviation of the Stokes parameters of the ten data sets. All the tables below follow the same logic. In Tab. 5 above, the standard deviation drops by two magnitudes for S_1 and S_2. S_0 and S_3 only change by a factor in the jitter corrected data set. Moreover, the DOP drops below 1 from the not corrected to the corrected case. This shows that the applied correction of the motor jitter is effective to a certain extend. Another observation made from Tab. 5 is that the measurement error in the corrected case is magnitudes higher than the standard deviation.

3.3.8 Wave Plate Ripple

An intensity modulation of the test signal is observed, when it passes through a rotating QWP as shown in Sec. 3.2.3. To make sure, that the wave plate ripple observed in this polarimeter set-up is caused by the wave plate itself, several steps are taken. As a first step, several photo diodes are tested, while the rest of the set-up remains unaltered. Next, five different wave plates are tested, while keeping the remainder of the set-up unchanged. Exchanging the photo diodes has virtually no effect on the observed ripple, as expected. Exchanging wave plates, however, leads to characteristic alterations in the observed wave plate ripple. Moreover, a photo diode is rotated, while the rest of the set-up remains unchanged. Also, no significant changes in the intensity can be observed.

To make sure that the ripple is not caused by the self-designed rotation

mount, the wave plate is rotated with a precision rotation mount instead of the DC-motor and the self-made rotation mount. Here, the observation is made that one of the wave plate axis transmits a higher intensity than the other. Another parameter that is changed is the tilt of the wave plate in respect to the signal that enters. Varying this tilt leads to a variation of the height of the amplitudes of the modulated signal of about 5 %.

The results of the above variations of parameters in the set-up supports the idea that the wave plate ripple is caused by intrinsic properties of the wave plate. Fig. 10 shows the ripple spectra of WP1 and ZO-WP. The spectra are recorded as described in Sec. 3.2.3 above. From Fig. 10 it is observed, that each wave plate has its characteristic ripple spectrum. Moreover, the ripple spectrum of a wave plate changes in a somewhat unpredictable fashion over time. These observations are consistent with the findings of [12].

From Fig. 10, the observed intensity modulation is roughly 3% for the ZO-WP and 2 % for WP1. For the ZO-WP, this meets the specifications of the manufacturer, who states that inensity fluctuations of 1 to 4 % may be observed due to the Fabry–Pérot etalons inside the wave plate [4], since there is an anti-reflection coating with a rest reflectivity of 0.25 % on each surface of the two quartz crystals in the ZO-WP. The specifications of WP1, however, are unknown. From close investigation it can be seen, that WP1 is not an air-spaced wave plate but a crystal plate of some sort.

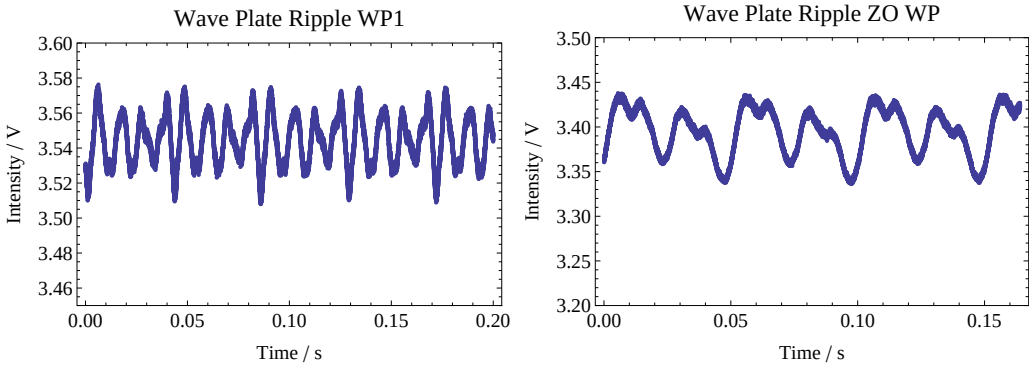

Figure 10: Recorded ripple spectra of WP1 and ZO-WP.

Fig. 11 below shows the ripple spectrum of the ZO-WP and a measurement of a test signal in the LVP state with the polarimeter set-up, where WP1

is the rotating QWP. Here, a periodic ripple in the signal recorded with the polarimeter is observed on the right side of Fig. 11. Interestingly, the periodicity of the wave plate ripple and the ripple in the LVP measurement are similiar. Following [5] ,the ripple in the signal recorded by the polarimeter is attributed to the wave plate ripple of the QWP itself.

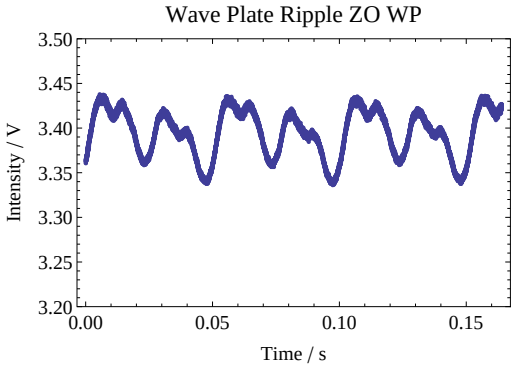

Figure 11: Effect of wave plate ripple on polarimeter measurements.

The effect of the wave plate ripple is tried to be corrected by Fourier transforming the ripple spectrum of the rotating QWP used the polarimeter [5]. The Fourier transform of the ripple spectrum is performed by the same algorithm that calculates the Fourier coefficients of the test signals recorded with the polarimeter set-up. This provides the A_{ripple}, B_{ripple}, C_{ripple} and D_{ripple} Fourier components of the wave plate's ripple spectrum, in analogy to the Fourier components of Eq. 5 . Next, the relative errors due to the ripple are calculated as: $\Delta B_{\text{ripple}} = \frac{B_{\text{ripple}}}{A_{\text{ripple}}}$, $\Delta C_{\text{ripple}} = \frac{C_{\text{ripple}}}{A_{\text{ripple}}}$ and $\Delta D_{\text{ripple}} = \frac{D_{\text{ripple}}}{A_{\text{ripple}}}$, where A_{ripple} is the DC term.

The Fourier components B,C and D of the test signals measured with the polarimeter are then corrected as follows: $B_{\text{corr}} = B - \Delta B_{\text{ripple}} \cdot A$. The C and D components are corrected correspondingly. Tab. 6 below shows the effects that the ripple correction has on the same data set of ten LVP measurements that has been evaluated in the motor jitter section of this chapter. Here, the uncorrected results are slightly better than the corrected results. Moreover, the corrected DOP of the corrected parameters is above 1. When the ripple correction is applied to similar data sets of -45LP, LHP states, the DOP may

even rise to values above 1.06 and produce relatively large deviations from the expected measurement values.

From these results, it is decided that this particular method for correcting the ripple does not work. To find the error, the wave plate ripple is re-examined in the laboratory. Now the observation is made, that the wave plate ripple changes in phase and amplitude, when the polarization state of the beam that enters the rotating QWP is changed. Moreover, there are other random changes in the wave plate ripple during the measurements that cannot be taken into account from a single measurement of the ripple before the polarization measurement. Therefore, the wave plate ripple is not removed from the recorded data with the above algorithm, since a more intricate reduction procedure hast to be developed.

This procedure would need to record the wave plate ripple during the polarization measurement, so that it could be corrected from the test signal with a transfer function. This would mean, that the one detector principle of the polarimeter set-up would have to be given up.

Table 6: Wave Plate Ripple Correction

	Ripple Not Corrected			Ripple Corrected		
	Mean Meas. Value / V	Mean Meas. Error / V	Std. Dev. / V	Mean Meas. Value / V	Mean Meas. Error / V	Std. Dev. / V
S0	1.2178	± 0.0160	0.0002	1.2250	±0.0160	0.0002
S1	-1.2161	±0.0160	0.0006	-1.2294	±0.0140	0.0006
S2	0.0102	±0.0149	0.0006	0.0103	±0.0150	0.0006
S3	0.0078	±0.0050	0.0005	0.0095	±0.0050	0.0001
DOP	0.9987	± 0.0196	0.0002	1.0037	±0.0201	0.0002

3.3.9 Signal Recording Length

To analyze the improvement made in the measurements results by recording longer signals, the data set of ten LVP measurements of 7 rotation periods from above is compared to a data set of ten measurements of 1 rotation period of the QWP. Next, the standard deviations of the results of both data sets are calculated for each Stokes parameter. the results are presented in Tab. 7 below. As expected, longer recording times reduce the standard deviation.

For S_1 and S_2 the improvement made is one magnitude. This is consistent with the findings of [6].

Table 7: Signal Length

	1 period			7 periods		
	Mean Meas. Value / V	Mean Meas. Error / V	Std. Dev. / V	Mean Meas. Value / V	Mean Meas. Error / V	Std. Dev. / V
S_0	1.2178	± 0.0160	0.0006	1.2178	±0.0160	0.0002
S_1	-1.2163	± 0.0140	0.0043	-1.2161	±0.0140	0.0006
S_2	0.0108	±0.0149	0.0043	0.0102	±0.0149	0.0006
S_3	0.0081	±0.0050	0.0007	0.0078	±0.0050	0.0005
DOP	0.9989	±0.0196	0.0003	0.9987	±0.0196	0.0002

3.3.10 Laser Stability, Wave Plate Wobble and Temperature

The effects of the laser stability and the wave plate wobble on the measurement of the Stokes parameters are not analyzed directly during this project. The stability of the laser intensity and wavelength are checked qualitatively with a power and wave meter and found to be sufficiently stable. The remaining statistical errors due to laser instability, wave plate wobble, unaccounted random motor jittering and temperature fluctuations are accounted for in the statistical analysis of data sets that contain ten independent measurements. A more profound analysis of the statistical error is limited by the recording equipment and the available calculation power.

4 Results

Table 8: Measurement Results ZO-WP.

	LVP			LHP			-45LP		
	Mean Meas. Val. / V	Mean Meas. Err./ V	Std. Dev. / V	Mean Meas. Val. / V	Mean Meas. Err. / V	Std Dev. / V	Mean Meas. Val. / V	Mean Meas. Err. / V	Std. Dev. / V
S_0	1.2178	± 0.0160	0.0002	1.3852	± 0.0179	0.0017	1.4444	± 0.0279	0.0010
S_1	-1.2161	± 0.0140	0.0006	1.4284	± 0.0159	0.0010	-0.0440	±0.0259	0.0003
S_2	0.0102	± 0.0149	0.0006	-0.0600	± 0.0257	0.0010	-1.4526	±0.0158	0.0003
S_3	0.0078	± 0.0050	0.0005	-0.0125	± 0.0050	0.0002	-0.0156	± 0.0050	0.0003
DOP	0.9987	± 0.0196	0.0002	1.0321	± 0.0217	0.0024	1.0062	± 0.0405	0.0006

Table 9: Measurement Results WP1.

	LVP			LHP			-45LP		
	Mean Meas. Val. / V	Mean Meas. Err./ V	Std. Dev. / V	Mean Meas. Val. / V	Mean Meas. Err. / V	Std Dev. / V	Mean Meas. Val. / V	Mean Meas. Err. / V	Std. Dev. / V
S_0	1.0607	± 0.0149	0.0008	1.0308	± 0.0145	0.0007	0.9651	± 0.0155	0.0007
S_1	-1.0617	± 0.0129	0.0002	0.9893	± 0.0125	0.0002	-0.0116	± 0.0135	0.0006
S_2	0.0116	± 0.0142	0.0002	0.0155	± 0.0137	0.0002	-0.9618	± 0.0123	0.0006
S_3	0.0050	± 0.0050	0.0000	0.0015	± 0.0050	0.0001	-0.0034	± 0.0050	0.0000
DOP	1.0010	± 0.0192	0.0002	0.9599	± 0.0185	0.0006	0.9967	± 0.0236	0.0003

The final measurement results with the ZO-WP and WP1 are presented in Tab. 8 and Tab. 9 above. For each DUT and each wave plate, a data set of ten single measurements has been analyzed. The tables above list the mean of the measured Stokes parameters and their standard deviations, as well as the mean of their cumulated measurement errors. In general, the measurement results are in good agreement with the theoretical expectations. The deviations of the measured Stokes parameters from the theoretically expected Stokes parameters are below 5% for both wave plates. The DOP is between 103 and 96 % for all measurement, which verifies the physical correctness of the measurements.

Moreover, the cumulated measurement error is up to two magnitudes higher than the standard deviations of the data sets. Noticeable are the relatively high measurement values for S_3 in the LHP and -45LP state of the ZO-WP. Other conspicuous value are S_2 in the LHP and S_1 in the -45LP measurement of the ZO-WP, because they are well outside the measurement error but have a relatively small standard deviation. The value of S_3 is above

the measurement error in all ZO-WP measurements. On the contrary, S_3 is in the limits of the estimated sampling error for the WP1 measurements.

Since the LHP measurement with the ZO-WP seems to be problematic, a closer look is taken at the data of one of the single measurements of the analyzed LHP data set. The left side of Fig. 12 below shows two periods of raw data of the single measurement. On the right side of Fig. 12, the corresponding sampled data points are shown. From the two graphs, it is evident that the data sampling method works accurately. Moreover, the signal recorded in the measurement shown below does not look like an ideal LHP signal.

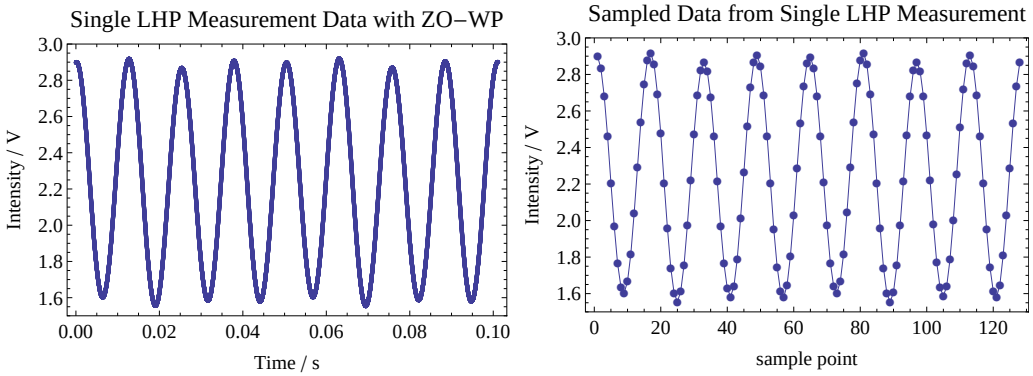

Figure 12: Single LHP measurement with ZO-WP.

The Stokes parameters are now calculated as described above and reinserted into Eq. 5. Fig. 13 below shows a plot of Eq. 5 with the calculated Stokes paremeters for the above LHP signal. The comparison with the measured signal in Fig. 12 above shows, that not all characteristics of the measured signal can be found in the calculated signal. The variations in the intensity in the lower amplitudes of the measured signal are also present in Fig. 13. The intensity variations in the upper amplitudes of the measured signal, however, are not shown in the calculated signal.

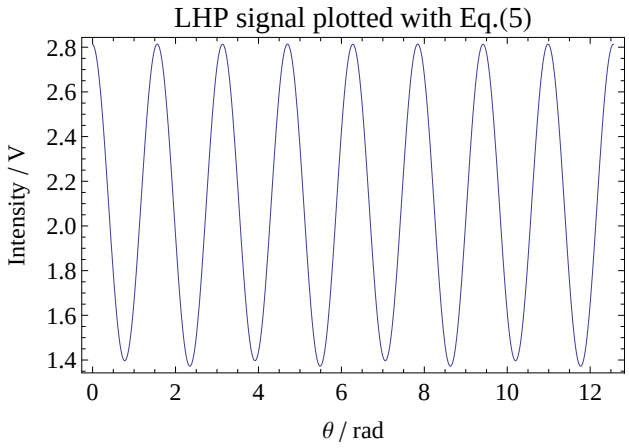

Figure 13

5 Discussion and Outlook

The low values of the standard deviations show that the statistical error in the measurements is small. On the contrary, the measurement error is one to two magnitudes higher than the corresponding standard deviation. This indicates, that the measurement error may be estimated too high.

The combination of a small standard deviation and a high deviation from the expected result, such as the S2 parameter in the LHP ZO-WP measurement, indicates that there are systematic errors in the measurement that have not been taken into account.

These systematic errors are believed to be connected to the wave plate ripple, since the recorded test signals show clear periodic deviations from the theoretically expected signals. Moreover, the misalignment of the encoder wheel with the rotation mount and unaccounted motor jittering may produce another systematic error.

An argument in favor of the wave plate ripple is the analysis of the LHP measurement in the above section (comp. Fig. 12). The ripple in the recorded test signal is also present in the sampled data. However, parts of the information of the sampled signal are lost in the calculation of the Stokes parameters with the Discrete Fourier transform algorithm in Mathematica. This may lead to an under-reporting of the systematic error that is believed to be

caused by the wave plate ripple in the calculated Stokes parameters. To what extend this is caused by possible under-sampling of the measured data or errors or the errors done in the Fourier transform itself, needs to be analyzed further. A method to check this, would be to use an encoder wheel with a higher resolution. Moreover, if the wave plate ripple would be introduced analytically as dynamic transmission coefficient of the rotating wave plate, it could produce more parameters and Fourier coefficients in the calculation of Eq. 5.

Contrarily, the LHP measurements of both wave plates show similar deviations in the DOP. This can be used as an argument in favor of the systematic error produced by unaccounted systematic motor jittering and the misalignment of the encoder wheel. This is supported further by the relatively large deviations in the S_1 parameters of the -45LP measurements of both wave plates. The deviations in S_2 for both LHP measurements would support this hypothesis further.

An argument against this is, however, that the DOPs of the LVP and -45LP measurements of both wave plates deviate from the expected value less than 1%. A systematic error caused by the motor and encoder wheel would be expected to cause a deviation in the DOP of the same value in the LVP and -45LP measurements as in the LHP measurements.

Another argument in favor of the wave plate ripple, is that the intensity modulation created by the wave plates themselves are up to 4%. In the ZO-WP LHP measurement, $S_2/S_0 \approx 0.04$. This means that the deviation in the LHP ZO -WP S_2 measurement is of approximately the same value as the intensity modulation in the signal that can be attributed to wave plate ripple. This is supported by the fact, that the wave plate ripple of the ZO-WP has a significant $\cos(4\omega \cdot t)$ component.

The above discussion shows, that the systematic errors in the set-up need to be further investigated. Since the wave plate ripple finds strong support in literature, it may be investigated further as a separate subject [2, 5]. First improvements to be made in the set-up are the installation of a higher resolution encoder wheel that is aligned perfectly with the center of the rotation mount. Moreover, the trigger signal should be created with a separate light

source.

Next, the wave plate ripple has to be studied further and an effective method to reduce it from the measurement data has to be found. To further reduce the errors made in the sampling process, the algorithm that dynamically adjusts the phase shift ϕ_{TT} between the fast axis of the QWP plate and the reference hole could be improved. One way to this would be to find ϕ_{TT} directly by Fourier transform and subsequently correcting the phase with ϕ_{TT} in the Fourier transform of the measured signals.

Moreover, an optically contacted or cemented QWP should be tested with the set-up, since it is suggested in [5] that these types of wave plates significantly reduce the wave plate ripple in polarimeters.

6 Conclusion

A rotating quarter wave plate Stokes polarimeter is designed, constructed and tested. The precision of the polarimeter is tested with an air-spaced quarter and an unknown wave plate, that is not air-spaced. The deviations from of the measurements from the expected values are below 5 %. A detailed data analysis is carried out and suggestions for the improvement of the polarimeter set-up are made. Wave plate ripple has been identified as a potential source for systematic errors in the measurement of the Stokes parameters.

7 Bibliography

References

[1] , D. C. B. Whittet, A. Chrysostomou, J. H. Hough, D. K. Aitken , G. S. Wright and P. F.Roche, "Spectropolarimetric Constraints", The Astrophysical Journal, vol. 512, pp. 224-229, Feb. 1999.

[2] D. K. Aitken and J. H. Hough, "Spectral Modulation, or Ripple, in Retardation Plates for Linear and Circular Polarization", Publications of the Astronomical Society of the Pacific, vol. 113, no. 788, pp.1300–1305, Oct. 2001.

[3] H. G. Berry, G. Gabrielse, and A. E. Livingston, "Measurement of the Stokes parameters of light," Appl. Opt. 16, pp.3200-3205, 1977.

[4] J. Borchers, Sales Representative LensOptics, E-mail from Sept. 13, 2001.

[5] J.H. Hough, 2005,"Polarimetry Techniques at Optical and Infrared Wavelengths", The future of photometric, spectrophotometric, and polarimetric standardization, C. Sterken (ed.), ASP Conference Series, Vol. 364, p. 3.

[6] V. A. Dlugunovich, L. V. Simonchik, V. N. Snopko, and O. V. Tsaryuk, "Goniophotometric laser Stokes-polarimeter", Measurement Techniques, vol.43, no.1, pp. 31-37, Jan. 2000.

[7] C. Flueraru, S. Latoui, J. Besse, P. Legendre, "Error Analysis of a Rotating Quarter-Wave Plate Stokes' Polarimeter," Instrumentation and Measurement, IEEE Transactions on , vol.57, no.4, pp.731-735, April 2008.

[8] D. Goldstein, *Polarized Light*. New York: Marcel Dekker, 2003.

[9] Wolfram Research, Inc., Mathematica, Version 8.0, Champaign, IL, 2011.

[10] P. C. Logofatu, ”Simple method for determining the fast axis of a wave plate”, Opt. Eng., vol. 41, no. 12, pp. 3316-3318, December 2002.

[11] P. A. Williams, “Rotating-wave-plate Stokes polarimeter for differential group delay measurements of polarization-mode dispersion,” Appl. Opt., vol. 38, no. 31, pp. 6508–6515, Nov. 1999.

[12] Laboratoire Astrophysique de Toulouse, "Polarisation Ripple induced by Halle Retarders ", available at: http://www.ast.obs-mip.fr/projets/espadons/pol/ripple.html, accessed on Sept. 20, 2011.

8 Appendix

The Allan variance is given as:

$$\begin{aligned} \langle \sigma^2(k) \rangle_t &= \frac{1}{2m} \sum_{s=1}^{m} \left(A_{s+1}(k) - A_s(k) \right)^2, \\ A_s(k) &= \frac{1}{k} \sum_{l=1}^{k} x_{(s-1)k+l}, \\ s &= 1, ..., m, \ m = m^{'} - 1. \end{aligned} \tag{13}$$

Here, the data set consists of m' independent measurements. The averaging is done over sub-ensembles of the size k.

Ich versichere, dass ich diese Arbeit selbständig verfasst und keine anderen als die angegebenen Quellen und Hilfsmittel benutzt sowie die Zitate kenntlich gemacht habe.

Bonn, den ..... Unterschrift .....